Absorption engineering of NbN nanowires deposited on silicon nitride nanophotonic circuits

V. Kovalyuk,[1,2] W. Hartmann,[1] O. Kahl,[1] N. Kaurova,[2] A. Korneev,[2,3] G. Goltsman,[2,4] and W. H. P. Pernice[1,*]

[1]*Institute of Nanotechnology, Karlsruhe Institute of Technology, 76344 Eggenstein-Leopoldshafen, Germany*
[2]*Department of Physics, Moscow State Pedagogical University, Moscow 119992, Russia*
[3]*Moscow Institute of Physics and Technology (State University), Moscow 141700, Russia*
[4]*National Research University Higher School of Economics, 20 Myasnitskaya Ulitsa, Moscow 101000, Russia*
[*]*wolfram.pernice@kit.edu*

Abstract: We investigate the absorption properties of U-shaped niobium nitride (NbN) nanowires atop nanophotonic circuits. Nanowires as narrow as 20nm are realized in direct contact with Si3N4 waveguides and their absorption properties are extracted through balanced measurements. We perform a full characterization of the absorption coefficient in dependence of length, width and separation of the fabricated nanowires, as well as for waveguides with different cross-section and etch depth. Our results show excellent agreement with finite-element analysis simulations for all considered parameters. The experimental data thus allows for optimizing absorption properties of emerging single-photon detectors co-integrated with telecom wavelength optical circuits.

OCIS codes: (130.3120) Integrated optics devices; (160.1050) Integrated optics materials; (220.4241) Nanostructure fabrication.

References and links

1. A. Gondarenko, J. S. Levy, and M. Lipson, "High confinement micron-scale silicon nitride high Q ring resonator," Opt. Express **17**(14), 11366–11370 (2009).
2. Y. Okawachi, K. Saha, J. S. Levy, Y. H. Wen, M. Lipson, and A. L. Gaeta, "Octave-spanning frequency comb generation in a silicon nitride chip," Opt. Lett. **36**(17), 3398–3400 (2011).
3. C. Xiong, W. H. P. Pernice, K. K. Ryu, C. Schuck, K. Y. Fong, T. Palacios, and H. X. Tang, "Integrated GaN photonic circuits on silicon (100) for second harmonic generation," Opt. Express **19**(11), 10462–10470 (2011).
4. Y. Zhang, L. McKnight, E. Engin, I. M. Watson, M. J. Cryan, E. Gu, M. G. Thompson, S. Calvez, J. L. O'Brien, and M. D. Dawson, "GaN directional couplers for integrated quantum photonics," Appl. Phys. Lett. **99**(16), 161119 (2011).
5. C. Xiong, W. H. P. Pernice, X. Sun, C. Schuck, K. Y. Fong, and H. X. Tang, "Aluminum nitride as a new material for chip-scale optomechanics and nonlinear optics," New J. Phys. **14**(9), 095014 (2012).
6. M.-C. Tien, J. F. Bauters, M. J. R. Heck, D. T. Spencer, D. J. Blumenthal, and J. E. Bowers, "Ultra-high quality factor planar Si_3N_4 ring resonators on Si substrates," Opt. Express **19**(14), 13551–13556 (2011).
7. E. S. Hosseini, S. Yegnanarayanan, A. H. Atabaki, M. Soltani, and A. Adibi, "High quality planar silicon nitride microdisk resonators for integrated photonics in the visible wavelength range," Opt. Express **17**(17), 14543–14551 (2009).
8. B. M. Zwickl, W. E. Shanks, A. M. Jayich, C. Yang, A. C. Bleszynski Jayich, J. D. Thompson, and J. G. E. Harris, "High quality mechanical and optical properties of commercial silicon nitride membranes," Appl. Phys. Lett. **92**(10), 103125 (2008).
9. B. Bhushan, *Springer Handbook of Nanotechnology*, 2nd ed. (Springer-Verlag, Heidelberg, 2007).
10. W. H. P. Pernice, C. Schuck, O. Minaeva, M. Li, G. N. Goltsman, A. V. Sergienko, and H. X. Tang, "High-speed and high-efficiency travelling wave single-photon detectors embedded in nanophotonic circuits," Nat Commun **3**, 1325 (2012).
11. C. Shuck, W. H. P. Pernice, O. Minaeva, M. Li, G. N. Goltsman, A. V. Sergienko, and H. X. Tang, "Matrix of integrated superconducting single-photon detectors with high timing resolution," IEEE Trans. Appl. Supercond. **23**(3), 2201007 (2013).

#194278 - $15.00 USD Received 23 Jul 2013; revised 9 Sep 2013; accepted 11 Sep 2013; published 19 Sep 2013

12. J. P. Sprengers, A. Gaggero, D. Sahin, S. Jahanmirinejad, G. Frucci, F. Mattioli, R. Leoni, J. Beetz, M. Lermer, M. Kamp, S. Hofling, R. Sanjines, and A. Fiore, "Waveguide superconducting single-photon detectors for integrated quantum photonic circuits," Appl. Phys. Lett. **99**(18), 181110 (2011).
13. R. H. Hadfield, M. J. Stevens, S. S. Gruber, A. J. Miller, R. E. Schwall, R. P. Mirin, and S. W. Nam, "Single photon source characterization with a superconducting single photon detector," Opt. Express **13**(26), 10846–10853 (2005).
14. R. E. Correa, E. A. Dauler, G. Nair, S. H. Pan, D. Rosenberg, A. J. Kerman, R. J. Molnar, X. Hu, F. Marsili, V. Anant, K. K. Berggren, and M. G. Bawendi, "Single photon counting from individual nanocrystals in the infrared," Nano Lett. **12**(6), 2953–2958 (2012).
15. P. Eraerds, M. Legre, J. Zhang, H. Zbinden, and N. J. Gisin, "Photon counting OTDR: advantages and limitations," J. Lightwave Technol. **28**(6), 952–964 (2010).
16. O. V. Minaeva, A. Fraine, A. Sergienko, A. Korneev, A. Divochiy, and G. Goltsman, "High resolution optical time-domain reflectometry using superconducting single-photon detectors," *Frontiers in Optics 2012/Laser Science XXVIII*, OSA Technical Digest (online) (Optical Society of America, 2012), paper FW3A.39.
17. C. Shuck, W. H. P. Pernice, X. Ma, and H. X. Tang, "Optical time domain reflectometry with low noise waveguide-coupled superconducting nanowire single-photon detectors," Appl. Phys. Lett. **102**(19), 191104 (2013).
18. N. Gisin, G. Ribordy, W. Tittel, and H. Zbinden, "Quantum cryptography," Rev. Mod. Phys. **74**(1), 145–195 (2002).
19. H. Takesue, S. W. Nam, Q. Zhang, R. H. Hadfield, T. Honjo, K. Tamaki, and Y. Yamamoto, "Quantum key distribution over a 40-dB channel loss using superconducting single-photon detectors," Nat. Photonics **1**(6), 343–348 (2007).
20. G. N. Goltsman, O. Okunev, G. Chulkova, A. Lipatov, A. Semenov, K. Smirnov, B. Voronov, A. Dzardanov, C. Williams, and R. Sobolevski, "Picosecond superconducting single-photon optical detector," Appl. Phys. Lett. **79**(6), 705–707 (2001).
21. A. Korneev, Y. Vachtomin, O. Minaeva, A. Divochiy, K. Smirnov, O. Okunev, G. Goltsman, C. Zioni, N. Chauvin, L. Balet, F. Marsili, D. Bitauld, B. Alloing, L. Li, A. Fiore, L. Lunghi, A. Gerardino, M. Halder, C. Jorel, and H. Zbinden, "Single-Photon Detection System for Quantum Optics Applications," IEEE J. Sel. Top. Quantum Electron. **13**(4), 944–951 (2007).
22. A. Semenov, G. Goltsman, and A. Korneev, "Quantum detection by current carrying superconducting film," Physica C **351**(4), 349–356 (2001).
23. C. Schuck, W. H. P. Pernice, and H. X. Tang, "Waveguide integrated low noise NbTiN nanowire single-photon detectors with milli-Hz dark count rate," Sci Rep **3**, 1893 (2013).
24. A. J. Kerman, E. A. Dauler, W. E. Keicher, J. K. W. Yang, K. K. Berggren, G. Gol'tsman, and B. Voronov, "Kinetic-inductance-limited reset time of superconducting nanowire photon counters," Appl. Phys. Lett. **88**(11), 111116 (2006).
25. Y. Korneeva, I. Florya, A. Semenov, A. Korneev, G. Goltsman, "New generation of nanowire NbN superconducting single-photon detector for mid-infrared," IEEE Trans. Appl. Supercond. **21**(3), 12022857 (2011).
26. X. Hu, "Efficient superconducting-nanowire single-photon detectors and their applications in quantum optics" PhD thesis, MIT (2011), *http://hdl.handle.net/1721.1/63073*

1. Introduction

Nanophotonic circuits allow for realizing complex optical functionality on a chip and enable the assembly of functional devices with many optical components in a scalable fashion. By exploiting established fabrication routines originally developed for the electronics industry, high-quality optical networks can be realized. While such circuits have been demonstrated very successfully using silicon as a waveguiding material, recently alternative materials have been investigated that overcome some of the shortcomings of silicon. In particular materials with a wider bandgap are desirable, as they allow for reduced free-carrier absorption and a broader transparency window which also covers wavelengths in the visible spectral region. In particular nitride based semiconductors such as silicon nitride [1,2], gallium nitride [3,4] and aluminum nitride [5] are attractive due to their compatibility with CMOS fabrication.

Waveguides based on Si_3N_4 provide low optical absorption in the infrared [6] and visible [7] wavelength region as well as good mechanical properties [8,9]. A large difference in refractive index between the Si_3N_4 and its cladding layers (air and SiO_2) allows for creating compact and flexible waveguides for nanophotonic circuits that highly concentrate the optical mode power within the waveguides. Tight confinement of the electrical fields is particularly important for the fabrication of hybrid systems, as for example integrated photonic-superconducting circuits, where the coupling efficiency of evanescent modes to a nearby

#194278 - $15.00 USD Received 23 Jul 2013; revised 9 Sep 2013; accepted 11 Sep 2013; published 19 Sep 2013

detector plays a critical role [10–12]. Such circuits are promising for use in both classical and quantum optical technologies, including characterization of quantum emitters [13,14], optical time domain reflectometry (OTDR) [15–17], quantum key distribution [18,19] and other tasks where several key requirements have to be met simultaneously: compact design, high quantum efficiency, broad spectral range and high timing resolution. One of the main elements of such circuits is a superconducting single-photon detector (SSPD) [20,21], which is realized by U-shaped NbN nanowires atop of a nanophotonic waveguide [10]. The detection mechanism of such devices is based on the transition from the superconducting to the normal state upon the absorption of a single photon, which leads to the creation of a localized hot-spot [22]. On the one hand it is necessary to obtain as much absorption as possible in the nanowire. On the other hand the dimensions of the nanowires are restricted by the hot spot size and cannot be made arbitrarily large without loss of detection efficiency [23]. Thus an increase in speed, quantum efficiency and spectral range of such detectors can be achieved by reducing the length and width of nanowires, at the cost of reduced absorption of incoming photons. In the first case this is due to the resulting decrease in the kinetic inductance of the nanowire [10,24], in the second case due to an increasing size of the hot spot with respect to the nanowire width [23,25].

Here we present a detailed study of the absorption coefficient of U-shaped NbN nanowires on top of Si_3N_4 waveguides for the relevant geometry parameters of the whole nanophotonic system. Our aim is to maximize the absorption efficiency while maintaining a minimal cross-section of the nanowire. We systematically vary the nanowire geometry and determine the absorption coefficient using on-chip balanced detection. Through transmission measurements in the telecom C-band we obtain the absolute absorption value in dependence of wavelength, which allows for extracting the normalized absorption coefficient per unit length. The measured values are in good agreement with absorption parameters extracted from finite-element simulations. Our results provide design guidelines for obtaining desired absorption values for a given detector geometry.

2. Device design and absorption engineering

In order to determine the absorption coefficient we measure transmission through on-chip waveguides with NbN nanowires fabricated on top. A schematic view of fabricated structures is shown in Fig. 1(a). For variation of the waveguide geometry we use two silicon substrates with different thickness of the waveguiding layer, deposited onto a buffered oxide layer with lower refractive index. The first class of substrates includes 3300nm SiO_2 and 330nm Si_3N_4, the second class 2600nm SiO_2 and 450nm Si_3N_4. The thickness of the underlying oxide is adjusted for maximizing the coupling efficiency into the fabricated circuits. On both platforms we pattern a matrix of nanophotonic circuits which consists of 264 elements and covers 9x9 mm^2 wafer area. An optical image of several devices placed on chip is shown in Fig. 1(g).

Each nanophotonic circuit includes two equal waveguide arms with the same length of about 360μm. One arm is used as the reference waveguide for light without any nanowire; the other arm is equipped with a U-shaped NbN nanowire on top. The waveguides are terminated with three focusing grating couplers with a coupler separation of 250μm among them, connected via a 50:50 Y-splitter. The focusing grating couplers are used to couple light from optical single mode fibers onto the chip and vice versa. The period and fill factor of these grating couplers were optimized for 1550nm wavelength and provide coupling efficiency of 19% for 450nm Si_3N_4 and 17% for 330nm Si_3N_4, respectively. We also experimentally optimized the geometric parameters of the 50:50 Y-splitter, to obtain even splitting ratio. In the optimized devices we obtain division of the incoming mode with an uncertainty below 0.5%. A schematic view of the nanowire on top of the waveguide is shown in Fig. 1(b). Here we also present the parameters which are varied during the absorption measurements. The length (l_{nw}), width (w_{nw}), and gap (g_{nw}), are the varied geometrical parameters of the

#194278 - $15.00 USD Received 23 Jul 2013; revised 9 Sep 2013; accepted 11 Sep 2013; published 19 Sep 2013

nanowires. We define the nanowire gap as the clear distance between two wires (indicated by the red line in Fig. 1(b)). The cross-section of the Si_3N_4 waveguides is adjusted by varying the width (w_{wg}) and height (h_{wg}).

Numerical analysis of mode propagation and nanowire absorption is carried out through finite-element simulations with COMSOL MultiPhysics and presented in Figs. 1(c)-1(f), using material parameters as given in [26]. In Figs. 1(c) and 1(e) we show the fundamental TE-like mode for the two studied substrate materials, where the optical mode is strongly confined inside the waveguide. In the presence of the NbN nanowire the evanescent tail of the guided mode is strongly coupled to the NbN wire (see Figs. 1(d) and 1(f)).

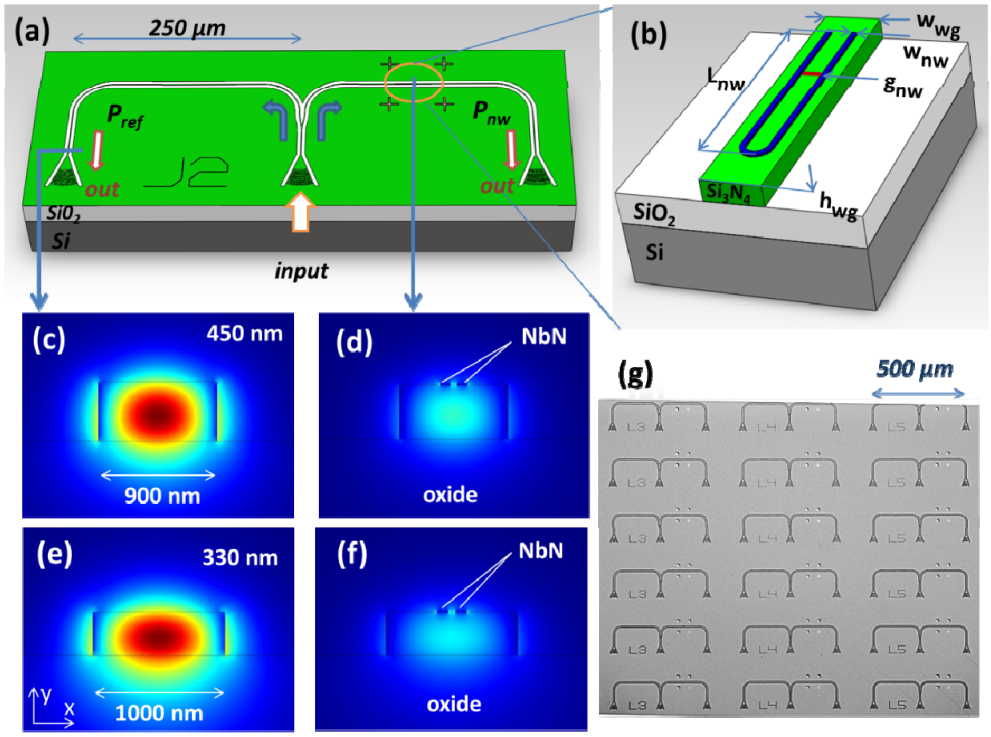

Fig. 1. (a) Schematic view of one nanophotonic device. (b) Cross-section of a nanophotonic waveguide covered with a U-shaped NbN nanowire. (c) Simulated distribution of the electric field in the x-direction (TE-like mode) for 1550nm wavelength and 450x900nm Si_3N_4 waveguide. Light intensities are shown in linear color scale. (d) Simulated distribution of the TE-like mode for 1550nm wavelength and 450x900nm Si_3N_4 waveguide in the NbN nanowire covered region. (e) Simulated distribution of the electric TE-like mode for 1550nm wavelength and 330x1000nm Si_3N_4 waveguide. (f) Simulated distribution of the TE-like mode for 1550nm wavelength and 330x1000nm Si_3N_4 waveguide in the NbN nanowire covered region. (g) Optical micrograph of a matrix of devices on a chip.

Using COMSOL we extract the complex refractive index of the propagating mode. From the imaginary part of the refractive index n_i the absorption coefficient can be directly extracted using the expression $\alpha = 4.34\ (4\pi n_i / \lambda)$, in units of dB/µm.

In addition to the design shown in Fig. 1(b) the absorption properties of nanowires deposited on ridge waveguides were investigated. In such waveguides only half of the 450nm Si_3N_4 was etched down as illustrated in Fig. 2(c). This type of waveguide provides further flexibility in adjusting the waveguide width, since single mode guiding is also possible for narrow ridges. Furthermore, by optimizing the focusing grating couplers we found that the maximum of coupling efficiency occurs at a different combination of a grating period and fill

#194278 - $15.00 USD Received 23 Jul 2013; revised 9 Sep 2013; accepted 11 Sep 2013; published 19 Sep 2013

factor for fully and half etched structures. Figures 2(e) and 2(f) show the spectra of transmission measured from the reference arm of nanophotonic devices for both cases. Half etched structures (FHWH = 35nm) have wider coupling bandwidth as compared with fully etched (FHWH = 24nm) for approximately the same coupled power. For this reason structures based on ridge waveguides can be more attractive for the realization of phase-sensitive devices where it is desirable to have a operational spectral range as wide as possible.

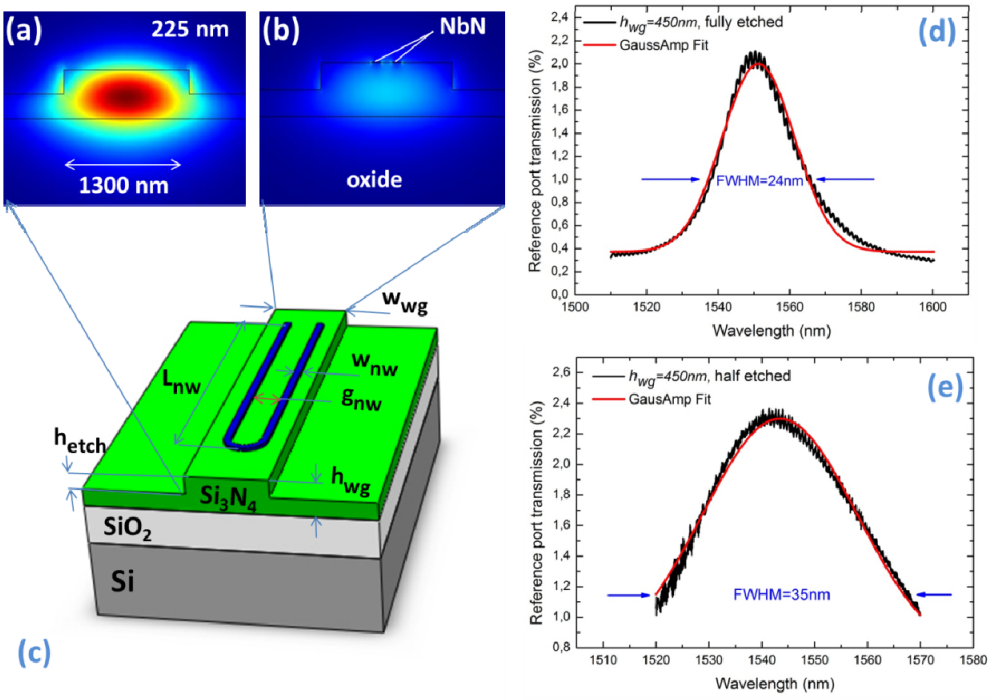

Fig. 2. (a) The simulated distribution of the electric field in the x-direction (TE-like mode) for 1550nm wavelength and a 225x1300nm Si_3N_4 waveguide cross-section. The field profile is shown in linear color scale. (b) The simulated distribution of the TE-like mode for 1550nm wavelength and 225x1300nm Si_3N_4 waveguide in the NbN nanowire covered region. (c) Schematic view of a half etched nanophotonic waveguide with a U-shaped NbN nanowire on top. (d) Transmission spectrum of the reference port of a fully etched device. (e) Transmission through a partially etched device, showing increased coupling bandwidth.

3. Device fabrication and measurement setup

For device fabrication we employ a multi-layer thin film platform. High-quality silicon wafers were covered by buried oxide (SiO_2), low pressure chemical vapor deposited (LPCVD) Si_3N_4 and sputtered NbN ultrathin films. The sheet resistance of as-deposited 4nm NbN film was measured as 400-500 Ohm/sq on the two wafers used in the experiments.

The process of nanophotonic circuit fabrication includes three steps of electron-beam lithography with marker search and subsequent alignment. In the first step electron-beam lithography with the positive resist polymethyl methacrylate (PMMA) is used to realize markers for the alignment of subsequent nanowire and waveguide patterns. Then a 4nm Cr adhesion-layer and a 50nm thick Au-film is evaporated, thus realizing clearly visible gold alignment markers after lift-off in acetone. Then a second e-beam lithography step for defining the nanowires is carried out using 3% high resolution hydrogen silsesquioxane (HSQ) resist. Reactive ion etching (RIE) in CF_4 chemistry was chosen for forming the NbN nanowires. Figures 3(e)-3(g) show a scanning electron microscope (SEM) image of resulting nanowires with different width. We realize nanowire widths down to 20nm. Note that the

#194278 - $15.00 USD Received 23 Jul 2013; revised 9 Sep 2013; accepted 11 Sep 2013; published 19 Sep 2013

wires are still covered by residual HSQ resist after dry etching. The last step of electron beam lithography is used to define optical waveguide structures. For this step we use the positive e-beam resist ZEP520A and reactive ion etching in CHF_3 chemistry to transfer the written structures into the Si_3N_4waveguide layer. SEM images of a fabricated nanophotonic device and its main components are presented in Figs. 3(a)-3(d). After removing the ZEP resist, NbN nanowires are still protected by a thin layer of HSQ with thickness about 30-40nm as observed by atomic force microscope (AFM). AFM images of several devices are presented in Fig. 4, showing that the nanowire geometry is highly uniform with a surface roughness below 2nm rms.

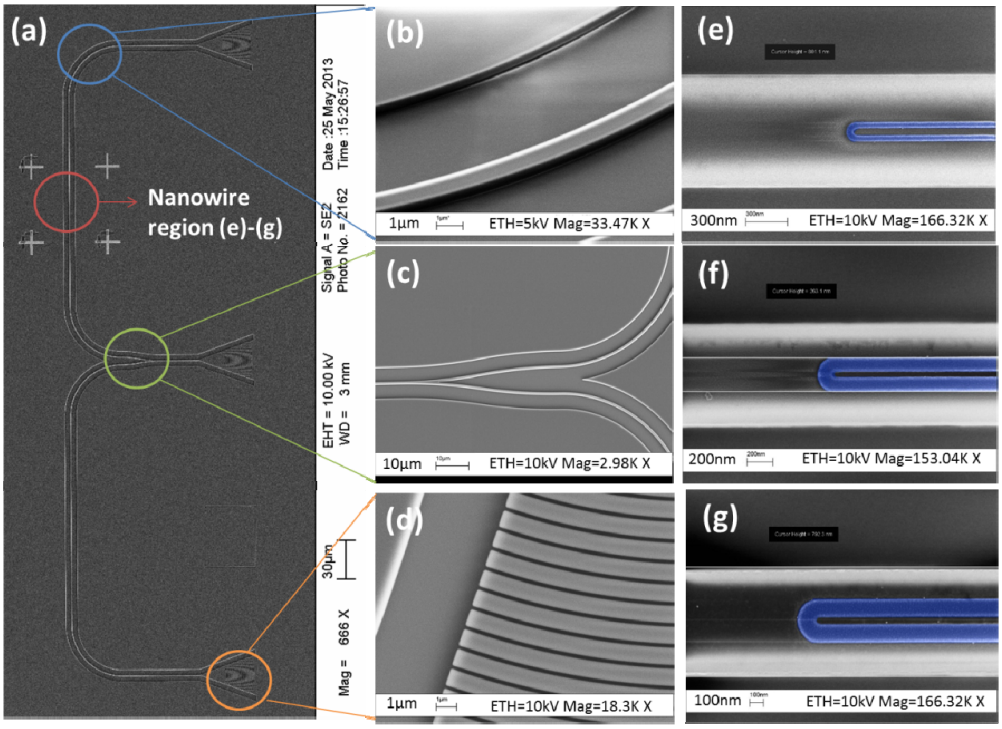

Fig. 3. (a) SEM image of a fabricated nanophotonic circuit consisting of focusing grating couplers, a 50:50 Y-splitter and alignment marks. (b) SEM image of the central element of a nanophotonic device (the waveguide). (c) SEM image of the Y-splitter. (d) SEM image of a portion of the focusing grating coupler. (e)-(f) SEM images with false colors of U-shaped NbN nanowire atop of Si_3N_4 waveguide with different width (27, 95, 120 nm, respectively).

For measuring the absorption rate of the nanophotonic devices we use a flexible alignment procedure in an optical fiber-based experimental setup. The fabricated chip with all devices is placed on a computer controlled xyz-θ stage which is equipped with piezo picomotors (New Focus 8752/8753). The minimum step size of the picomotors is less than 30 nm, which allows for precise alignment of the grating couplers under an optical fiber array. To measure transmission we use a continuously swept, tunable wave laser (New Focus TLB-6600, 1510-1620nm), manual polarization controllers (THORLABS FPC030) and a fiber array with a fiber-to-fiber spacing of 250µm, corresponding to the separation of the on-chip grating couplers. Light incoming from an optical fiber passes through optimized grating couplers into the on-chip single mode waveguide. The light is coupled from the fiber array into the central coupling port. The 50:50 splitter routes half of the coupled light to the reference port and the other half to the nanowire region. At the output grating couplers from reference port (P_{ref}) and nanowire port (P_{nw}) we record the transmitted signal and measure it with two low-noise

#194278 - $15.00 USD Received 23 Jul 2013; revised 9 Sep 2013; accepted 11 Sep 2013; published 19 Sep 2013

calibrated photodetectors (New Focus, 2117) simultaneously. Alignment and transmission measurements are carried out for all devices on the fabricated chips to allow for statistical analysis.

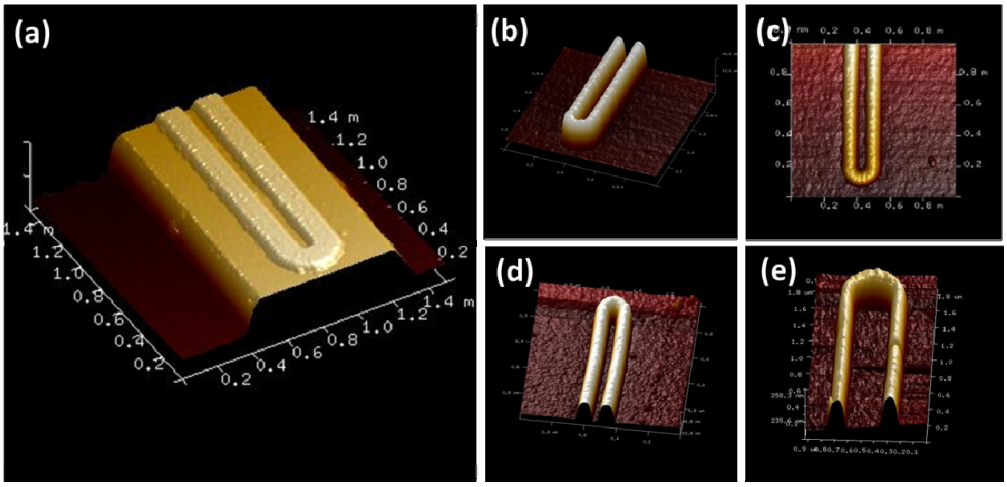

Fig. 4. (a) AFM picture of a NbN nanowire atop a Si_3N_4 waveguide. (b)-(e) AFM pictures of fabricated NbN nanowires with different parameters (gap and wire width). The fabricated wires are still covered with residual HSQ ebeam resist after dry etching.

4. Results

For calculating the absorption coefficient from experimental data we compare the transmitted optical signals at the reference and the output port. Then the actual absorption value is obtained using the following equation:

$$\alpha = \frac{10}{l_{nw}} \lg\left(\frac{P_{nw}}{P_{ref}}\right), \tag{1}$$

where α is the absorption coefficient [dB/μm], l_{nw} – length of the nanowire, P_{nw} – measured power from the arm with nanowire region, P_{ref} – reference power from arm without any nanowire.

4.1 Fully etched nanophotonic devices

In Fig. 5(a) we show the dependence of the absorption coefficient versus waveguide width for the two silicon nitride substrates used in our experiments (red: 330nm, black: 450nm). The squares and circles are the experimental data, while solid lines show the results of the numerical simulations as described above.

The absorption rate versus waveguide width has smooth peak dependence. We find lower absorption rates for waveguide widths below 1000nm (for 330nm Si_3N_4) or 850nm (for 450nm Si_3N_4), respectively. This is the results of the waveguide cut-off condition for 1550nm input wavelength which dominates with decreasing waveguide width. For wider waveguides the absorption coefficient decreases also due to the profile of the optical mode which shows weaker evanescent coupling to the nanowire with increasing waveguide width. The maximum value of the nanowire absorption coefficient is 0.34 ± 0.02 dB/μm, obtained for a waveguide height of 330nm and a width of 1000 nm. For a waveguide height equal to 450nm we find a maximal absorption rate of 0.27 ± 0.01 dB/μm which occurs around 850nm.

The most drastic increase of the absorption coefficient is shown in Fig. 5(b). Here the waveguide width and the spacing between the nanowires are kept approximately equal for each Si_3N_4/SiO_2 platforms, while the width of the nanowire itself is varied. The measured

#194278 - $15.00 USD Received 23 Jul 2013; revised 9 Sep 2013; accepted 11 Sep 2013; published 19 Sep 2013

absorption coefficient follows a power low, where the best fit yields a dependence of $|\alpha| = 1.8 \times 10^{-6} x^{2.7}$ for 330nm Si_3N_4 and $|\alpha| = 1.7 \times 10^{-6} x^{2.6}$ for 450nm Si_3N_4. The dependence of the absorption coefficient versus nanowire width is not surprising because an increase in the width of the strip increases the area of overlap between the evanescent waveguide mode and the nanowire. As in Fig. 5(a) the numerical simulations (solid line) are in good agreement with the experimental data. When we fix all the parameters of waveguides and nanowires, except for the gap between the strips U-shaped nanowire, we obtain the relationship shown in Fig. 5(c). The results show that the absorption rate decreases with increasing nanowire gap, because the nanowire is displaced from the center of waveguide where the intensity of the evanescent mode is the highest.

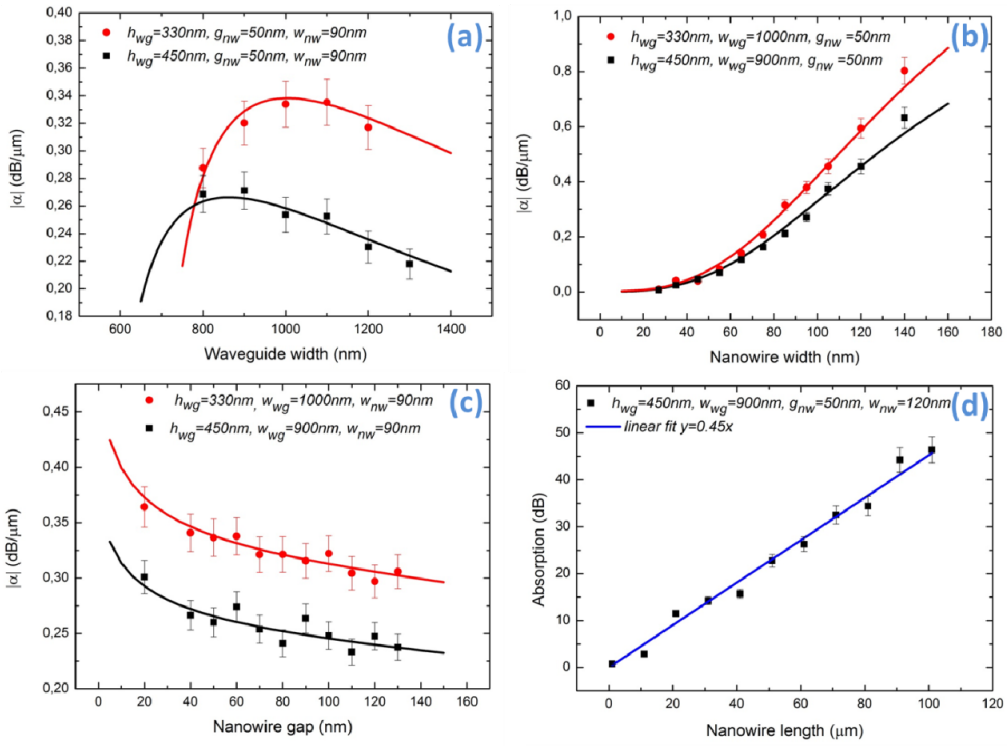

Fig. 5. Absorption coefficient of U-shaped NbN nanowire versus different geometrical parameters nanophotonic devices. For all graphs solid line is a simulation and dots are measured data. Red data rely to Si_3N_4 330nm, SiO_2 3300nm, black data relay to Si_3N_4 450nm, SiO_2 2600nm platform. (a) Dependence of absorption coefficient versus waveguide width. (b) Dependence of absorption coefficient versus NbN nanowire width. (c) Dependence of absorption coefficient versus NbN nanowire gap. (d) Dependence of absorption coefficient versus NbN nanowire length.

The dependence of the absorption coefficient versus nanowire gap can be approximated as $|\alpha| = 0.50x^{-0.1}$ for 330nm Si_3N_4 and $|\alpha| = 0.42x^{-0.11}$ for 450 nm Si_3N_4. We further observe a linear dependence of nanowire absorption versus length as shown in Fig. 4(d). Overall, the measured absorption rate is lower than obtained for U-shaped NbN nanowires on silicon on insulator (SOI) [5]. This is predominantly due to the larger waveguide cross section necessary for lower refractive index contrast waveguides.

4.2 Half etched nanophotonic devices

For the half etched waveguide structures we find qualitatively similar behavior of the absorption as for the fully etched waveguides mentioned before. Measured data for several

#194278 - $15.00 USD Received 23 Jul 2013; revised 9 Sep 2013; accepted 11 Sep 2013; published 19 Sep 2013

nanowire parameters is presented in Fig. 6. Unlike the fully etched structures with 450nm of Si_3N_4 (where the maximum of absorption occurs at 850nm waveguide width) we find the highest absorption coefficients for a wider waveguide width between 1000nm and 1100nm. The absorption increases with the width of the nanowire and decreases with the gap.

Given a U-shaped nanowire geometry of 60nm width and 100nm gap we find the maximum absorption for a waveguide width of 1000nm at 0.069dB/μm ± 0.003dB/μm. The dependence on the nanowire width can be fitted as $|\alpha| = 2.9 \times 10^{-6}\, x^{2.4}$ for a waveguide width of 1300nm and a gap of 100nm and x being the width of the wire. The dependence of the absorption coefficient on the nanowire gap can be approximated as $|\alpha| = 0.14x^{-0.12}$. The absorption coefficient versus nanowire length for a waveguide width of 1000nm, nanowire width of 60nm and nanowire gap of 100nm can be approximated as $|\alpha| = 0.068x$, showing the expected linear behavior. Nevertheless, for both device configurations (half etched and fully etched, respectively) we find good agreement with the numerical predictions.

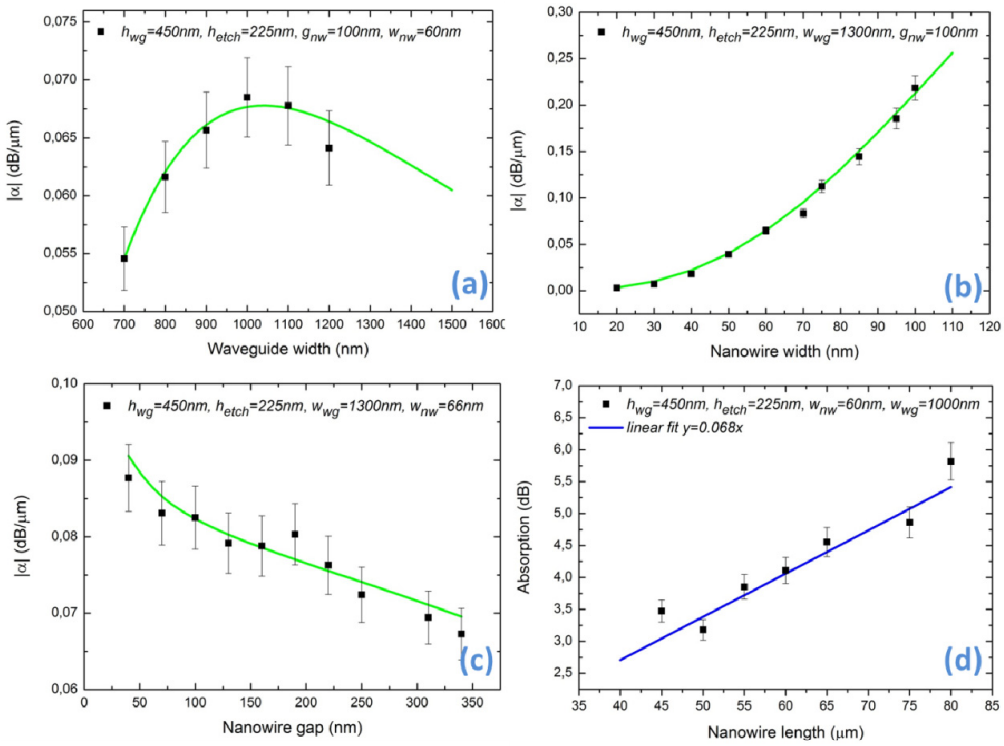

Fig. 6. Absorption coefficient of U-shaped NbN nanowire versus different geometrical parameters of nanophotonic devices. For all graphs the solid line is the simulation data and dots are measured data of a half etched Si_3N_4 450nm, SiO_2 2600nm platform. (a) Dependence of the absorption coefficient versus waveguide width. (b) Dependence of the absorption coefficient versus NbN nanowire width. (c) Dependence of the absorption coefficient versus NbN nanowire gap. (d) Dependence of the absorption coefficient versus NbN nanowire length.

A direct comparison between the two configurations from measured data is not always possible, due to different waveguide geometry, nanowire width, gap etc. of the fabricated devices. However, we can directly compare absorption coefficients for fully and half etched waveguides extracted from numerical simulations for the same geometry of nanowires. We find a significant decrease of the maximum value of absorption coefficient of half etched structures absorption (0.19 dB/μm) compared to the fully etched (0.27 dB/μm) devices on 450nm Si_3N_4. We attribute this with pulling down the optical mode further into the substrate (see Figs. 2(a), 2(b)). Therefore the evanescent field overlapping with the nanowires is

#194278 - $15.00 USD Received 23 Jul 2013; revised 9 Sep 2013; accepted 11 Sep 2013; published 19 Sep 2013

weaker than on structures where the waveguide is fully etched, which leads to the mode being located approximately in the center of the waveguide.

We estimate the uncertainty in the measurement of the absorption coefficient, which results from the error of the 50:50 splitting ratio, the optical power measurements error and uncertainty in determining the geometrical parameters of nanowires. To decrease measurement errors associated with the uncertainty of the geometric size of the resulting nanophotonic devices, the parameters of the structures were measured by electron scanning electron microscope (SEM) and atomic force microscope (AFM) after fabrication. We estimate a 5% total error during our absorption measurements, measuring a large number of devices and excluding differ greatly from the average value. The calculated error bars are shown in Figs. 5, 6.

5. Conclusions

We measured the absorption coefficient for U-shaped NbN nanowires directly placed on top of nanophotonic devices. By varying the nanowire geometrical parameters in width, nanowire separation and length we found that the maximum absorption rate occurs for a waveguide of 1000nm width for one configuration (330nm Si_3N_4, 3300nm SiO2) and at 850nm for the other configuration (450nm Si_3N_4, 3300nm SiO2). Changing the nanowire width and gap with fixed waveguide width around the maxima we found increasing absorption rate with increasing width and decreasing gap between the NbN nanowires. Similar behaviour we also observed for devices that were only half etched into ridge waveguides. Nevertheless, in this geometry we measure a lower absorption coefficient for the same geometry of the nanowires. Our measured values are in good agreement with finite-element analysis simulations, which therefore provide a rapid evaluation tool for nanowire absorption. The data can be used for engineering hybrid nanophotonic-superconducting circuits for integrated classical and quantum applications.

Acknowledgments

V. Kovalyuk acknowledges support by Russian Presidential Scholarship for studying abroad and by the Ministry of Education and Science of the Russian Federation, contract #14.B25.31.0007 of 26 June 2013. W. H. P. Pernice acknowledges support by DFG grant PE 1832/1-1 and the Helmholtz society through grant HIRG-0005. We also acknowledge support by the Deutsche Forschungsgemeinschaft (DFG) and the State of Baden-Württemberg through the DFG-Center for Functional Nanostructures (CFN) within subproject A6.4. The authors further wish to thank B. Voronov and N. Titova for the deposition of the NbN thin films and Silvia Diewald for assistance in device fabrication. We acknowledge support by the Deutsche Forschungsgemeinschaft and Open Access Publishing Fund of Karlsruhe Institute of Technology.